Calibration of electrons and photons with the ATLAS detector, and its impact on ATLAS precision measurements

C. Becot

EPJ Web of Conferences **95**, 04004 (2015)
DOI: 10.1051/epjconf/ 20159504004

Impact of ATLAS electromagnetic calibration on precision measurements

Cyril Becot[1, a] on behalf of the ATLAS collaboration

[1] *Laboratoire de l'accélérateur linéaire, Orsay*

Abstract. Since the discovery of the Higgs boson a lot of effort has been devoted to the measurement of its properties. One of its key parameter is its mass, which has been measured by the ATLAS detector at the LHC. For this measurement a precision calibration of the ATLAS electromagnetic calorimeter is required. The details of this calibration as well as the current understanding of the detector will be described. The measurement of m_H and the impact of the calibration will be described.

1 Introduction

The discovery of the Higgs boson associated to the Brout-Englert-Higgs mechanism has opened new perspectives in particle physics. A completely new sector of nature now need to be mapped, and this will be dominated by a measurement of the properties of the newly discovered particle. In the standard model the mass of the boson, m_H, is the only free parameter. Therefore, although m_H is not a strong test of new physics effects, it has to be known precisely to allow the observation of deviations from the standard model. This is especially true for branching ratios of the Higgs going into two vector bosons, which are rising quickly with respect to m_H.

Only two channels allow for a precise measurement of m_H with the current statistics : the $H \to \gamma\gamma$ and $H \to ZZ^* \to 2l2l'$ (with l,l'=e or μ) channels. They both require a very good understanding of electrons and photons energies, which is mainly achieved by a precise calibration of the electromagnetic (EM) calorimeters. After a short description of the ATLAS EM calorimeter, we will see in details how this calibration is achieved in ATLAS, and in a last part we will describe how the uncertainties from the EM calibration affect m_H. Although the $H \to 2l2l'$ channel will be discussed briefly, the main focus will be on the $H \to \gamma\gamma$ channel as it is more sensitive to all the details of the calibration.

The last measumement if m_H in the $H \to \gamma\gamma$ channel has been published in [1], and the underlying calibration in [2]. They will both be described below.

2 Description of the ATLAS electromagnetic calorimeter

A detailed description of the whole ATLAS detector has already been published in [3] and we will only focus on its EM calorimeter. It is a sampling calorimeter, made out of lead absorbers and using liquid argon (LAr) as active material. A schematic view of this subdetector is displayed in fig. 1.

a. e-mail: becot@lal.in2p3.fr

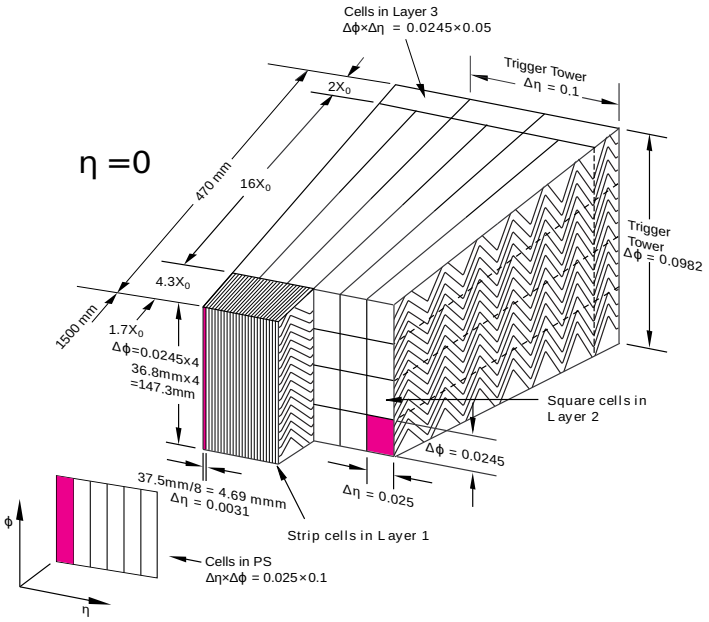

Figure 1. Schematic view of the central part of the EM calorimeter [4]

When electrons enter the calorimeter they emit photons in the absorbers, while photons will convert into e^+e^- pairs. These processes will happen in cascade hence creating an electromagnetic shower that will ionize the LAr. An electric field is applied to the LAr so that the ionization electrons will drift toward an electrode, creating an electric signal that has a triangular shape. The nominal high voltage applied to create this field is 2000 V in the central part of the detector.

This calorimeter is built as three layers in depth, plus one pre-sampler (PS) up to $|\eta| = 1.8$. The three layers have different thickness and cell segmentations. The bulk of the energy ($\approx 80\%$) is measured in the second layer, only a small energy fraction going to the last layer for photons from $H \rightarrow \gamma\gamma$.

After a first amplification, the electric signal will go through an electronic bipolar shaping whose main property is to give an output signal with a null integral. This gives an average cancellation of the impact of pile-up on the energy as the signal of several contiguous bunch crossing will be summed, but shifted with regard to each other. Therefore even with pile-up electrons and photons have on average the same energy as without pileup. But the number of pile-up vertices follow a Poisson distribution hence creating fluctuations of the ambient energy on an event-by-event basis has an impact on the energy resolution of the detector.

The electronic shaper has three gain ranges as outputs. The analog signals are stored and digitized after a level-1 trigger. Using three gain ranges with a 12bit analog to digital converter ensures good precision over the full dynamic range.

3 Improvements of the Monte-Carlo based calibration

It is not possible to measure the full energy of electrons and photons as there are energy losses in passive material, lateral energy leakage, before/after the calorimeter that need to be accounted for. To do this we rely on the simulation, which is our only way to know either the true energy of the incident

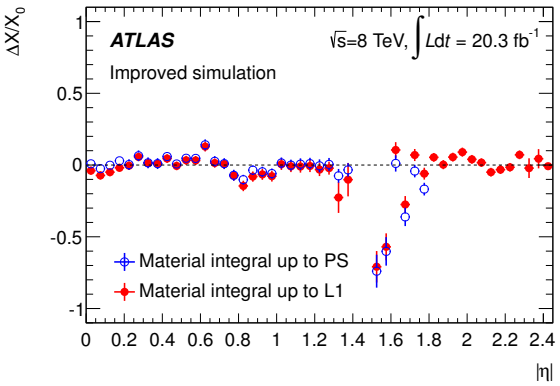

Figure 2. Relative difference of material budget between the data and the current simulation [2]

particle or all its energy deposits on an event by event basis. There has been sizeable improvements in the ATLAS simulation as well as in our parametrization of energy losses with respect to the previous result.

3.1 Material budget in front of the calorimeter

The pre-requisite to any performant energy reconstruction is a good knowledge of the material budget in front of the EM calorimeter. A dedicated method based on the ratio of energies in the first two layers has been used to determine it. The basic idea is that additional material will imply earlier showers. The sensitivity of this method was derived by comparing the nominal simulation to simulation samples with additional material. Applying it to data, it was afterward possible to find the difference of material distribution between simulation and data.

There are two locations where additional material may be found : before the PS, and between the PS and the first layer. In order to distinguish these, two probes have been used : unconverted photons with a veto on PS energy for the part after the PS, and electrons which are sensitive to the whole material budget. Any discrepancy between the simulation and the data was cross-checked on maps of the detector and on pictures of its construction before being implemented in the new simulation. The difference of material distribution between the new simulation and the data is shown in fig. 2. There are still a few differences between data and MC. The biggest one, at the beginning of the endcap, would correspond to an excess of material in the simulation with respect to the data. Almost all improvements between the former and the new detector description are addition of material that was missing.

Whenever a significant discrepancy between the data and simulation still exists, it is taken as the uncertainty on the material budget. Otherwise the uncertainty comes from the material extraction method.

3.2 Particle energy reconstruction

In the past ATLAS has been using explicit parametrizations of the energy losses, built on the simulation, to reconstruct the energy of the incident particle. This has not been used for the last results where a boosted decision tree (BDT), trained to get $\frac{E_{reco}}{E_{true}} = 1$, has been developed.

It takes as input the energy deposits in each layer and in the PS, in clusters of cells whose sizes depend on the particle type and its position in the detector. It also takes into account the depth of the electromagnetic shower, the position of the particle and, for converted γ, informations from the conversion tracks. Both the position in the ATLAS frame and with respect to the center of the most central cell are considered, as particles hitting closer to the edge of a cell will usually have a bigger energy leakage outside of there clusters. As the shower shapes are not well described by our simulation (see part 5.2), they could not be implemented in this BDT that is trained on Monte Carlo.

It is important to note that we have three BDT : one for electrons, one for unconverted photons and one for converted photons.

4 Pre-corrections for energy response on data

4.1 Corrections for non-uniformities and time-dependence

Using either the radial variations of the reconstructed Z boson mass (m_Z) in $Z \rightarrow ee$ events or of $\frac{E}{p}$ for electrons from $W \rightarrow e\nu$ events two main sources of non-uniformity in the energy response of the calorimeter have been identified. They are corrected in an ad-hoc way that flattens m_Z along ϕ.

The first effect is linked to the effect of gravity on the central part of the EM calorimeter. It has been built as 16 independent modules in ϕ, and under their weight the modules on top have a larger inter-module gap than those on the bottom. This creates a drop of energy response near the inter-module regions for the top part, that we have been able to correct for.

The second effect is linked to improperly corrected non-nominal high-voltage (HV), which in most cases corresponds to short-circuits. Usually such problems can be corrected assuming that the current in the electrodes is zero. This is not true anymore in case of short-circuits where there is a clear drift of the HV from its measured value at the power supply to 0 at the point of the short-circuit.

Z and W events also allowed to correct for a small time-dependence of the response. The PS response suffered from increasing noise with increasing pile-up. This was dealt with by decreasing the PS HV in september 2012 which gave a different energy response between the two periods, that we have also been able to correct for.

Once these corrections are applied we recover a very good time stability and uniformity of the energy response. This is shown in figs. 3 and 4.

4.2 Correction for an apparent non-linearity

As a cross-check it was decided to study the Z mass in two categories : those electrons with at least one cell of the second layer in medium gain (MG), and the others where every second layer cell is read in high gain (HG). A difference of energy response between these two categories was observed, and a correction aiming to equalize the response between the two is applied. This effect has been associated with an uncertainty that has the same size as the correction. It is quite likely that this categorization also implies an underlying relabelling of another effect.

4.3 Intercalibration of the layers

The next part will describe the determination of the absolute energy scale of the EM calorimeter, which is needed to take into account the remaining discrepancies between data and MC. But in order to apply only one energy scale we need to make sure that the various layers have the same scale. It was observed that the response of the first layer differs by $\approx 3\%$ from the one of the second layer, and

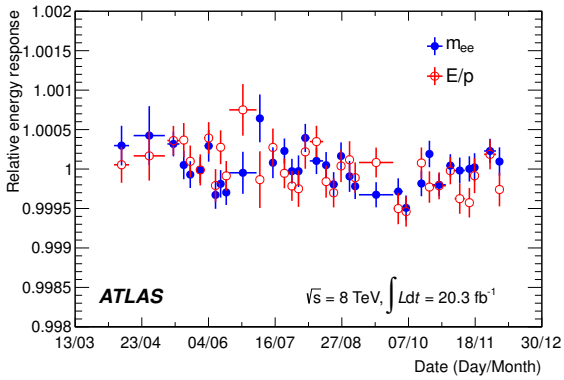

Figure 3. Time stability of energy response, measured by fitting M_Z or the most probable value of $\frac{E}{p}$ for electrons from Ws, in time in 2012 [2]

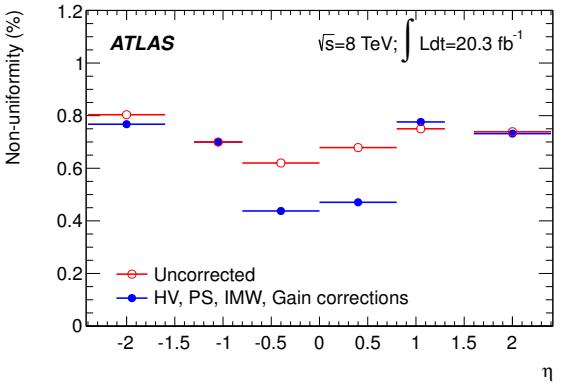

Figure 4. Non-uniformity of the energy response, measured as the RMS of M_Z in ϕ, after substraction of the expected statistical fluctuations. This is shown before and after the pre-corrections are applied [2]

hence one of the two need to be recalibrated. At the energies we were interested in this first run (up to 100 GeV for the Higgs), the third layer does not matter.

An inter-layer calibration $\alpha_{1/2}$ has been derived using muons in $Z \to \mu\mu$ events. Their big advantage is that they are insensitive to material in front of the calorimeter, and that their energy deposits in a layer are proportional to its depth. The obvious drawback is that they deposit only a few hundred MeVs in each layer, hence not being much above the noise. $\alpha_{1/2}$ is set to equalize $\frac{E_1}{E_2}$ between data and MC and its value can be seen in fig. 5. Although this could have been applied to any of the two layers, it was decided to apply it to the second as it is the one with the large variation of $\alpha_{1/2}$ at the beginning of the endcap.

Once the response of these layers is properly equalized one can set the energy scale of the presampler, which is a different detector, using a method based on $\frac{E_1}{E_2}$, described in [2].

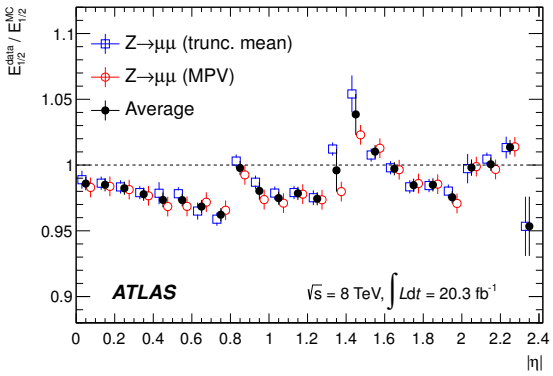

Figure 5. Values of $\alpha_{1/2}$ measured using two methods to define the average energy of muons in each layers [2]

5 EM calorimeter energy scale

5.1 Determination of the energy scale

The absolute energy scale of the EM calorimeter, α, is then set using $Z \rightarrow ee$ events, and its values can be seen in fig. 6. The data could still have a few problems that need to be corrected while the simulation is considered to be perfect. Therefore the energy response of the calorimeter on data need to be corrected by modifying the energy through $E \rightarrow (1 + \alpha)E$. This is done by aligning the M_Z peak on data to the one from the simulation. At the same time the energy resolution of the detector is determined. This is needed to smear the MC as it does not have all the non-uniformity and time-dependent effects that degrade the resolution.

This way of setting the absolute energy scale ensures that every effect is taken into account for 40 GeV electrons, and they should not suffer from any uncertainty other than the ones from the scale setting method. These uncertainties come from a lot of cross-checks, for instance comparing two methods to set the scales orincreasing the background. Every other uncertainty on the energy measurement appears either as a non-linearity or as an electron-to-photon extrapolation problem.

To make sure that we have not missed any uncertainty at low p_T a cross-check using J/Ψ events to set the scale is presented in [2]. The variation of the scale from $Z \rightarrow ee$ events to the one from $J/\Psi \rightarrow ee$ events is everywhere within our uncertainty. Therefore we feel confident that our energy scale is valid in a large p_T range and that no source of non-linearity has been forgotten.

5.2 Extrapolation to photons

The extrapolation of the energy scale to photons is less trivial as they are sensitive to other effects.

The first one comes from problems in the conversion reconstruction. As mentioned in part 3.2 if the photons are converted or not, we use a different calibration, because they may not be sensitive to the same effect (e.g. unconverted photons are insensitive to material). But if we treat a converted photon as an unconverted one it will have its energy slightly shifted. This would not be a problem if the rate of misclassification was the same in data and MC, but the modelling is not perfect. A small uncertainty on the energy, between $0.01\% - 0.1\%$ arises from this effect.

The second problem comes from the simulation of shower shapes which are known to be wider in data than in MC. For electrons the difference of energy leaking out of the clusters is taken into account

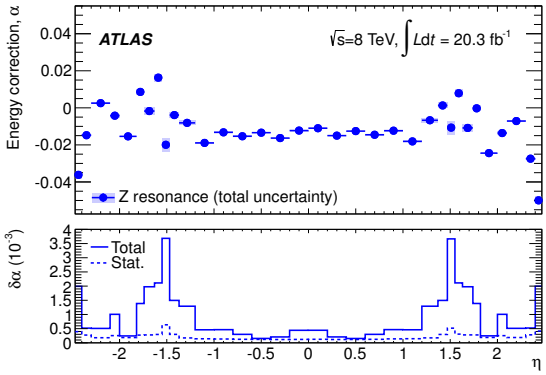

Figure 6. Energy scale from the $Z \to ee$ [2]

by the energy scales, but any difference of this mismodeling between electrons and photons would not be covered. This mismodeling is slightly bigger for photons - especially for converted photons. This gives an uncertainty on the energy measurement that ranges from 0.03% for unconverted photons in the most central region to 0.45% for converted at the end of the barrel.

6 Impact on the Higgs mass measurement

6.1 Description of the $H \to \gamma\gamma$ channel

The $H \to \gamma\gamma$ channel is characterized by a narrow mass peak corresponding to the signal on top of a smooth and falling background. We will only discuss the uncertainties from the calibration as they are the dominant ones. The full details of all the uncertainties can be found in [1, 2].

The mass is determined through a profiled likelihood fit. In order to improve its performance the dataset is split into several categories, depending on the kinematics of the diphoton pair, the position of the photons and whether or not one of them is converted. The signal model is a sum of a Crystal Ball and a wide gaussian, while the background shape depends on the category. The parameters of the background are all fitted to data.

The uncertainties are implemented as constrained nuisance parameters in the likelihood. All the calibration uncertainties are using a Gaussian constraint. In order to determine the variance of the nuisance parameters the signal Monte Carlo is used. Each uncertainty is propagated to the energy measurement of this Monte Carlo. This biased sample is then fitted with the full signal model, and the difference between the nominal and biased sample gives the variance of the nuisance parameters.

This fit gives us $m_H^{\gamma\gamma} = 125.98 \pm 0.42$ (stat) ± 0.28 (syst) GeV, where the dominant systematic is the apparent LAr cell non-linearity, followed by the systematics on material and the layer inter-calibration. This is a remarkable achievement as this is a decrease of more than a factor 2 of our uncertainty with regard to the previous result [5].

6.2 Combined result

The $H \to 4l$ channel has also seen quite a big improvement as the systematic uncertainty is now 10 times below the statistical one, at $m_H^{4l} = 124.51 \pm 0.52 \pm 0.06$ GeV. The most striking improvement

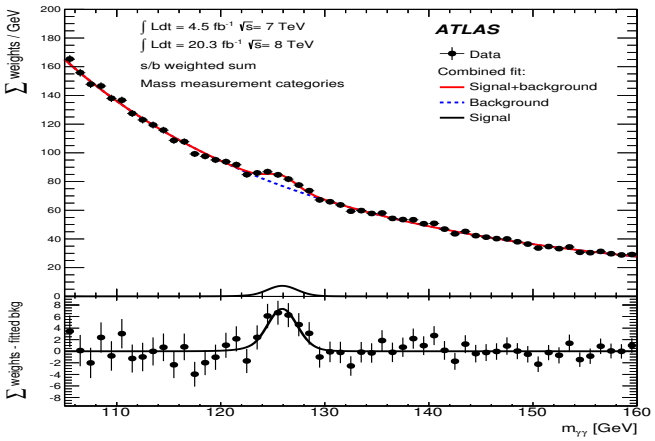

Figure 7. Invariant mass distribution of the diphoton system. Bottom plot is after background substraction [1]

is in channels with electrons as the electron energy scale is not anymore the dominant source of uncertainty.

We combined the results of the two channels, by multiplying there likelihoods. The final combined results is $m_H = 125.36 \pm 0.37 \pm 0.18$ GeV, and the two channels are compatible at the level of 2σ. The difference in m_H between the two channels is not very significant and is fully compatible with a statistical fluctuation.

7 Conclusion

The latest ATLAS results on the Higgs mass are a huge improvement with respect to the previous one. The calibration effort required to pave the way to this decrease in uncertainty gave us an outstanding understanding of our detector. There are still a few points that would profit from a deeper scrutiny. These were treated conservatively. But the current calibration is a good basis for future m_H measurements.

References

[1] ATLAS Collaboration, *Measurement of the Higgs boson mass from the $H \to \gamma\gamma$ and $H \to ZZ^* \to 4l$ channels in pp collisions at center-of-mass energies of 7 and 8 TeV with the ATLAS detector*, Phys. Rev. D. **90**, 052004

[2] ATLAS Collaboration, *Electron and photon energy calibration with the ATLAS detector using LHC Run 1*, http://arxiv.org/abs/1407.5063

[3] ATLAS Collaboration,*The ATLAS Experiment at the CERN Large Hadron Collider* (2008), JINST, **3** S08003

[4] ATLAS Collaboration, **Liquid Argon Calorimeter Technical Design Report**, CERN/LHCC/96-041 (1996)

[5] ATLAS Collaboration, *Measurements of the properties of the Higgs-like boson in the two photon decay channel with the ATLAS detector using 25 fb^{-1} of proton-proton collision data* (2013), ATLAS-CONF-2013-012, https://cds.cern.ch/record/1523698/